Published in final edited form as:
Circ J. 2011 ; 75(4): 834–843.

Intracellular Calcium and the Mechanism of Anodal Supernormal Excitability in Langendorff Perfused Rabbit Ventricles

Boyoung Joung, MD, PhD[1], **Hyung-Wook Park, MD, PhD**[1], **Mitsunori Maruyama, MD, PhD**[1], **Liang Tang, PhD**[1], **Juan Song, PhD**[1], **Seongwook Han, MD, PhD**[1], **Gianfranco Piccirillo, MD**[1], **James N. Weiss, MD**[2], **Shien-Fong Lin, PhD**[1], and **Peng-Sheng Chen, MD**[1]

[1]Krannert Institute of Cardiology and the Division of Cardiology, Department of Medicine, Indiana University School of Medicine, Indianapolis, Indiana

[2]Division of Cardiology, Department of Medicine and the Department of Physiology, David Geffen School of Medicine, UCLA, Los Angeles, California

Abstract

Background—Anodal stimulation hyperpolarizes cell membrane and increases intracellular Ca^{2+} (Ca_i) transient. This study tested the hypothesis that The maximum slope of Ca_i decline ($-(dCa_i/dt)_{max}$) corresponds to the timing of anodal dip on the strength-interval curve and the initiation of repetitive responses and ventricular fibrillation (VF) after a premature stimulus (S_2).

Methods and Results—We simultaneously mapped membrane potential (V_m) and Ca_i in 23 rabbit ventricles. A dip was observed on the anodal strength-interval curve. During the anodal dip, ventricles were captured by anodal break excitation directly under the S_2 electrode. The Ca_i following anodal stimuli is larger than that following cathodal stimuli. The S_1-S_2 intervals of the anodal dip (203 ± 10 ms) coincided with the $-(dCa_i/dt)_{max}$ (199 ± 10 ms, p=NS). BAPTA-AM (n=3), I_{NCX} inhibition by low extracellular Na^+ (n=3), and combined ryanodine and thapsigargin infusion (n=2) eliminated the anodal supernormality. Strong S_2 during the relative refractory period (n=5) induced 29 repetitive responses and 10 VF episodes. The interval between S_2 and the first non-driven beat was coincidental with the time of $-(dCa_i/dt)_{max}$.

Conclusions—Larger Ca_i transient and I_{NCX} activation induced by anodal stimulation produces anodal supernormality. Time of maximum I_{NCX} activation is coincidental to the induction of non-driven beats from the Ca_i sinkhole after a strong premature stimulation.

Keywords

anodal dip; anodal stimulus; intracellular calcium; Na^+-Ca^{2+} exchanger current

Introduction

The heart can be excited by either cathodal or anodal stimulation. The anodal threshold is higher than the cathodal threshold during late diastole.[1–3] As the S_1-S_2 intervals progressively shortens, the anodal threshold increases, then decreases, and then increases again during the relative refractory period (RRP) until the effective refractory period (ERP) is reached. The S_1-S_2 coupling interval associated with a transient reduction of anodal threshold is referred to as an anodal dip in the strength-interval (SI) curve.[4] The anodal dip

Corresponding author: Peng-Sheng Chen, MD, 1800 N. Capitol Ave, E475, Indianapolis, IN 46202., Phone : 317-962-9755, Fax: 317-962-0588, chenpp@iupui.edu.

Disclosures: None.

is also termed anodal supernormality, as the capturing threshold is less than expected for that S_1-S_2 coupling. Anodal dip may potentiate therisk of anodal pacing–induced ventricular fibrillation.[4] The absolute threshold values, however, may be either lower or higher than the diastolic threshold. A dip in SI curve is not observed during cathodal stimulation. We hypothesize that electrogenic Na^+-Ca^{2+} exchanger current (I_{NCX}), which progressively increases as membrane potential becomes more negative during repolarization, contributes to the occurrence of anodal dip in the SI curve. Because the timing of the anodal dip roughly corresponds to the vulnerable period of cardiac cycle,[4] we hypothesize that I_{NCX} activation also contributes to the mechanisms of ventricular vulnerability. While it is not feasible to measure real time I_{NCX} changes in intact ventricles, previous studies [5, 6] indicated that the rate of Ca_i decline ($-dCa_i/dt$) correlated well with measured I_{NCX}. Therefore, the $-(dCa_i/dt)_{max}$ is used as an estimate of the timing of the maximum Ca removal from NCX (peak I_{NCX}) during phase 3 repolarization.

If I_{NCX} activation is important in the anodal dip on the SI curve, then the timing of the anodal dip should be coincidental with the $-(dCa_i/dt)_{max}$. Similarly, if I_{NCX} activation is important in ventricular vulnerability, then the first non-driven beat that initiates repetitive responses or VF should also occur at the time of $-(dCa_i/dt)_{max}$. We performed simultaneous membrane potential (V_m) and Ca_i mapping in rabbit ventricles to test these hypotheses.

Methods

Langendorff-Perfused Rabbit Heart

This study protocol was approved by the Institutional Animal Care and Use Committee of Indiana University School of Medicine and the Methodist Research Institute, and conforms to the guidelines of the American Heart Association. We used 23 normal New Zealand white rabbits (3 to 5 kg). The rabbits were anesthetized with ketamine and xylazine. The chests were opened via medium sternotomy and the hearts were rapidly excised and immersed in cold Tyrode's solution (composition in mmol/L: 125 NaCl, 4.5 KCl, 0.25 $MgCl_2$, 24 $NaHCO_3$, 1.8 NaH_2PO_4, 1.8 $CaCl_2$, and 5.5 glucose). The ascending aorta was immediately cannulated and perfused with 37°C Tyrode's solution equilibrated with 95% O_2 and 5% CO_2 to maintain a pH of 7.4. Coronary perfusion pressure was regulated between 80 and 95 mm Hg. Two widely spaced bipolar electrodes were used for continuous pseudo-ECG monitoring. Duringoptical recordings, contractility was inhibited by 10–17 μmol/L of blebbistatin.[7]

Dual V_m and Ca_i Recordings

We used 0.5 mg of Rhod-2 AM (Molecular Probes) dissolved in 1 mL of dimethylsulfoxide containing Pluronic F-127 (20% wt/vol) to stain Ca_i. This solution was diluted in 300 ml of Tyrode's solution to achieve a final Rhod-2 concentration of 1.48 μmol/L. It was infused into the heart over a 10 min period. The heart was then stained again by direct injection of voltage sensitive dye (RH237, Molecular Probes) into the perfusion system. The double-stained heart was excited with laser light at 532 nm.[8] Fluorescence was collected using 2 cameras (MiCAM Ultima, BrainVision, Tokyo, Japan) at 2 ms/frame and 100X100 pixels with spatial resolution of 0.35x0.35 mm^2/pixel. The fluorescence induced by the laser illumination was obtained through a common lens, separated with a dichroic mirror (650 nm cutoff wavelength), and directed to the respective camera with additional filtering (715 nm long pass for V_m and 580 ± 20 nm for Ca_i).

Experimental Protocol

S_1 and S_2 were performed with 2 unipolar pacing electrodes (diameter 1.0 mm) on the left ventricle along the fiber direction. A left ventricular patch electrode was used as a reference

electrode. The distance of 2 unipolar pacing electrodes was within 5 mm. The electrode closer to the base of left ventricle was used for the S_1, and the other electrode on the anterior wall of left ventricle for S_2. The S_1 was cathodal with 6 ms pulse duration and twice diastolic threshold current. The S_1 pacing protocol consisted of an initial drive cycle of eight stimuli at a cycle length of 350 ms to overdrive the intrinsic heart rate. S_2 pulse duration was 6 ms for both cathodal and anodal polarities. Both S_1 and S_2 were delivered using a constant current stimulus isolator (A385, World Precision Instruments, Sarasota, FL). The pacing was initiated at S_1-S_2 interval of 250 ms with S_2 stimulus strength of 0.1 mA. The strength of S_2 was then gradually increased at 0.1 mA steps until it reached 1 mA, then at 0.5 mA steps until the stimulus captured the ventricles. At each S_1-S_2 interval, anodal and cathodal thresholds were determined by alternating the S_2 polarity. The S_1-S_2 interval was then progressively decreased at 10 ms steps and the same procedure was repeated until the SI curves were determined for both the anodal and the cathodal stimuli (Figure 1A).

In the first 14 hearts, the S_1-S_2 coupling interval associated with a transient reduction of anodal threshold was defined as an anodal dip in the SI curve. The period of non-anodal dip was defined by the S_1-S_2 intervals longer than the S_1-S_2 intervals comprising the anodal dip (Figure 1A). There was a 5-s to 10-s interval between pacing to allow adjustment of the S_2 strength. The RRP is the period (coupling intervals) associated with increased S_2 threshold. After the SI curves were determined, we delivered the S_2 during the RRP and progressively increased the strength of S_2 at 5 mA step until it reached 30 mA. The time of S_2 was marked by a light-emitting diode (LED) lamp, which was positioned in the mapped field. The same stimulator signal that triggered an S_2 pulse was used to trigger the LED lamp. The light artifact (black arrows on V_m optical map in Figure 1B) was used to document the timing of the S_2. We used BAPTA-AM (20 μmol/L) to chelate the Ca_i in 3 hearts.[9, 10] In additional 9 hearts, we performed the following interventions: (a) acute I_{NCX} blockade by rapidly substituting the Na^+ in the perfusate by Li^+ (n=3),[11, 12] (b) adding thapsigargin (3 μmol/L, n=3), ryanodine (10 μmol/L, n=1), or combined ryanodine and thapsigargin infusion (n=2). The SI curves were determined before and after these pharmacological interventions.

Data Analyses

The Ca_i and V_m traces were normalized to their respective peak-to-peak amplitude for comparison of timing and morphology (Figure 2A). Latencies were measured from the initiation of S_2 pulse (time zero) to the takeoff of V_m and Ca_i. To analyze the relationship between the anodal dip, the vulnerable period and Ca_i removal, we determined $-(dCa_i/dt)_{max}$ in the Ca_i transient tracing (black arrow, Figure 3D). Data are presented as mean ± SEM. Paired t tests were used to compare the time of $-(dCa_i/dt)_{max}$ and the mean anodal dip period for each heart studied. A p value of <0.05 was considered statistically significant.

Results

Anodal Dip and the SI curve

Figure 1A shows a typical example of anodal and cathodal SI curve. The anodal threshold had a dip when S_1-S_2 intervals were at 180 ms and 190 ms (red asterisks in Figure 1A). In this ventricle, the mean anodal threshold during the anodal dip (0.48 ± 0.1 mA) was less than the anodal threshold associated with longer S_1-S_2 intervals (0.72 ± 0.04 mA). For all 14 hearts studied, the anodal dip was located at a mean S_1-S_2 interval of 203 ± 10 ms. During this period, the anodal threshold (0.46 ± 0.30 mA) was significantly lower than cathodal one (0.79 ± 0.80 mA, p=0.04). Figure 1B shows the V_m and Ca_i optical ratio map snapshots at the time of S_2 delivery at different S_1-S_2 intervals. During anodal dip of 180 ms and 190 ms, the S_2 sites (arrows) were located near the area of largest Ca_i gradient, which was typically surrounded by areas of high Ca_i (red) and low Ca_i (blue) (supplementary Figure 1s). This

finding indicates that reduced anodal S_2 capturing threshold occurred to the cells with rapidly declining Ca_i. In contrast, the S_2 given outside the anodal dip period was associated with a uniformly low Ca_i (blue color in Ca_i maps at 200–250 ms S_1-S_2 intervals in Figure 1B). Figure 1C shows the V_m and Ca_i tracings recorded from the S_2 site (cross mark in Figure 1B) during S_1 pacing interval of 350 ms. These tracings also show that the anodal dip coincided with the rapidly declining Ca_i and V_m.

Differential Effects of Anodal and Cathodal Stimulation on Ca_i Elevation

We assigned the peak and lowest V_m fluorescence level of the last S_1 paced beat as 1 and 0 arbitrary unit (AU), respectively. The anodal S_2 given during the anodal dip results in more V_m hyperpolarization (0.035 ± 0.04 AU) than the cathodal S_2 (0.072 ± 0.055 AU, p=0.001). We assigned the peak Ca_i fluorescence level of the last S_1 paced beat as 1 AU. The Ca_i levels measured 30 ms after anodal and cathodal S_2 were 0.50 AU and 0.43 AU, respectively (Figure 2A). In all anodal dips studied (n=20), the Ca_i levels 30 ms after anodal stimuli were significantly higher than cathodal ones (0.63 ± 0.16 AU vs. 0.58 ± 0.19 AU, p=0.005). The Ca_i level 40 ms after anodal stimulus was also significantly higher than cathodal one (0.72 ± 0.14 AU vs. 0.68 ± 0.16 AU, p=0.001, Figure 2B). These findings reproduced the results of a previous report,[13] and support the notion that there are differential effects of anodal and cathodal stimulation on Ca_i transients.

The Anode-Break Excitation During Anodal Dip

For S1-S2 interval longer than that associated with anodal dip, the mode of excitation was anodal break (n=14). We next verified that the mode of excitation during anodal dip was anodal-break excitation. Figure 3 shows the anode-break excitation with anodal stimulus of 0.4 mA during the dip (S_1-S_2 interval of 190 ms). The earliest excitation started directly from the S_2 site (site 1) at the trailing edge of anodal stimulus (arrow, Figure 3A), compatible with break excitation. Figure 3B shows an isochronal map with times of activation (in ms) marked on selected isochrones, with the onset of S_2 as time zero. Figure 3C shows corresponding V_m and Ca_i fluorescence snapshots, showing that excitation started from the S_2 site (arrow) and propagated faster along the fiber direction than across the fiber direction. This finding of anodal break excitation was consistently observed during the anodal dip in all hearts studied.

Maximum Rate of Ca_i Removal and the Anodal Dip

We differentiated the Ca_i transient trace to measure dCa_i/dt at the S_2 site. Figure 3D shows the dCa_i/dt curve and V_m traces for S_1-paced beats at the S_2 site. The dCa_i/dt values were the highest during phase 1 and the lowest during the phase 3 of the action potential. $-(dCa_i/dt)_{max}$ (arrow) occurred when S_1-S_2 coupling interval was 180 ms, which was during the anodal dip in this heart.

For all hearts studied (n=14), $-(dCa_i/dt)_{max}$ occurred an average of 199 ± 10 ms after the S_2, which coincided with the average time of anodal dip (203 ± 10 ms after S_2, p=0.09, supplementary Figure 2s). In all hearts studied, the anodal threshold during the dip was 0.28 ± 0.14 mA. The anodal threshold with longer S_1-S_2 coupling intervals was 0.34 ± 0.20 mA.

The Effects of Calcium Chelating Agent on Anodal Dip

To explore further the relationship between anodal dip and the Ca_i transient, we compared SI curves before and during BAPTA-AM infusion. In normal hearts, the Ca_i transient maintained from 0.97 ± 0.02 AU to 0.95 ± 0.03 AU (− 2 %, n=7, p=0.34) after the 1 hour of study. In contrast, the Ca_i transient decreased from 0.97 ± 0.02 AU to 0.70 ± 0.06 AU (− 28 %, n=3, p=0.001) 1 hour after BAPTA-AM infusion (Figure 3s). Figure 4A shows the

changes of SI curves from baseline (broken lines) and after >1 hr BAPTA-AM infusion (solid lines). In all 3 hearts studied, BAPTA-AM abolished the anodal dip (Figure 4s). The anodal ERPs at baseline and during BAPTA-AM infusion were 170 ± 10 ms and 167 ± 21 ms, respectively (p=0.74). After BAPTA-AM infusion, it was not easy to find the $-dCa_i/dt$ max (Figure 4B).

The Effects of I_{NCX} block and SR Calcium Handling on Anodal Dip

To block I_{NCX},[11, 12] rapidly substituting the Na^+ in the perfusate by Li^+ was used in 3 hearts. Anodal dip disappeared after blocking I_{NCX} (Figure 5A). Thapsigargin infusion, which blocks SR calcium uptake, did not change the timing of anodal dip (Figure 5B). The S_1-S_2 coupling interval associated with anodal dips was 182 ± 19 ms before and 183 ± 12 ms after the addition of thapsigargin (P=0.74). However, ryanodine (SR Ca release block, Figure 5C)) or combined ryanodine and thapsigargin infusion (Figure 5D) eliminated anodal dip.

Maximum Rate of Ca_i Removal, Ca_i sinkhole and Ventricular Vulnerability

We mapped a total of 39 episodes of repetitive responses or VF induced by a single anodal stimulus. The stimulus strength was 20 ± 9 mA and the S_1-S_2 coupling intervals were 165 ± 16 ms. This coupling interval was significantly shorter than the coupling intervals associated with the anodal dip (p=0.001). In all 39 episodes with repetitive responses or VF, the timing of the V_m rise that initiated the repetitive response or VF was 123 ± 33 ms after S_2, which was coincidental with the $-(dCa_i/dt)_{max}$ at that site (121 ± 34 ms, p=0.07). (Note that the $-(dCa_i/dt)$max in this case was measured on the S_1 beats during stable pacing, not measured on the S_2 beat.) The S_1-S_2 coupling interval of repetitive response was longer than that of VF (171 ± 15 ms, vs. 150 ± 9 ms, p=0.001). The level of S_2 energy was not different between repetitive response and VF (19 ± 9 mA, vs. 25 ± 6 mA, p=0.08).

A Ca_i sinkhole [8, 13, 14] is a region with low (<50% of the average fluorescence) Ca_i surrounded by regions of normal or high Ca_i. On optical maps, the Ca_i sinkhole is a region of blue color surrounded by red color. Figure 6 shows the activation within the Ca_i sinkhole. A Ca_i sinkhole (asterisk, Panel A2) was observed 78 ms after the S_2, at a site of virtual cathode. Panels A3-A4 show progressive Ca_i elevation that started from the left side of the sinkhole and filled the whole sinkhole area. This Ca_i elevation did not induce sufficient V_m changes to induce a propagated action potential. Figure 6B shows the activation map which ends at the sinkhole site. Figure 6C shows the optical signals and the dCa_i/dt at the Ca_i sinkhole. The onset of V_m (blue arrow) was coincidental with the $-(dCa_i/dt)_{max}$ (black arrow).

Figure 7 shows repetitive responses induced by a 10 mA anodal stimulus given with a S_1-S_2 interval of 190 ms. A Ca_i sinkhole (asterisk, Panel A2) was observed 60 ms after the S_2, at a site of virtual cathode. Panels A3-A5 show progressive Ca_i elevation that started from the left side of the sinkhole and moved slowly towards the right side of the sinkhole (while arrows). In contrast to Figure 6, a wavefront, which was initiated at the Ca_i sinkhole at 106 ms after S_2, propagated to the remainder of the mapped region (Figure 7B). Figure 7C shows the optical signals and the $(dCa_i/dt)_{max}$ at the Ca_i sinkhole. The onset of V_m (blue arrow) was coincidental with the $-(dCa_i/dt)_{max}$ (black arrow).

Figure 8 shows a typical example of VF induced by a S_2. Figure 8A shows the Ca_i sinkhole (asterisk, Panel A2) produced by 30 mA anodal stimulus at the S_1-S_2 interval of 160 ms. There was also slow elevation of Ca_i that started from the left side of the sinkhole and propagated towards right side. There was then V_m elevation 105 ms after the S_2. The wavefront then propagated away from that site (Figure 8B). Ca_i sinkhole was observed again

at the same site (asterisk, panel A4). Figure 8C shows the optical signals and the $(dCa_i/dt)_{max}$ at the Ca_i sinkhole. The onset of V_m (blue arrow) was coincidental with the $-(dCa_i/dt)_{max}$ (black arrow).

Discussion

Our study demonstrates that the anodal dip on the SI curve occurred coincidentally with the $-(dCa_i/dt)_{max}$. Furthermore, the timing of the V_m rise that initiated the repetitive response or VF was also coincidental with the $-(dCa_i/dt)_{max}$. These findings suggest that I_{NCX} activation most likely played a role in anodal dip of the strength-interval curve, and may have contributed to the induction of non-driven beats from the Ca_i sinkhole induced by a strong premature stimulation.

Pacemaker Current (I_f) and Anodal Excitation

Ranjan et al.[15, 16] proposed that hyperpolarization-activated "funny" current (I_f) is responsible for anodal break excitation. However, hyperpolarization-activated cation channel mRNA expression was not observed in rabbit ventricle.[17] Thus, additional mechanisms are needed to explain the mechanisms of anodal dip. Our data suggest that maximal I_{NCX} activation is the factor that determines the timing of anodal supernormality.

Effects of BAPTA-AM

A significant finding of this study relates to the abolition of anodal dip when the Ca_i transient was suppressed with BAPTA-AM. This observation highlights the importance of the Ca_i transient in sculpting the electrophysiological environment during late phase 3 to promote anodal dip. The anodal dip coincided with the maximum rate of Ca_i removal $-(dCa_i/dt)_{max}$ even after pretreatment with thapsigargin, which blocks the SR Ca^{2+} reuptake. Since previous studies [5, 6] have documented that inward current through I_{NCX} is maximal at $-(dCa_i/dt)_{max}$, the stimulation of inward I_{NCX} by the combined effects of persistently elevated Ca_i and the progressively more negative membrane voltage during late phase 3 is likely to be a major factor antagonizing repolarization, and thereby decreasing the excitation threshold, during the anodal dip. The effects of BAPTA-AM strengthened this conclusion.

Ventricular Vulnerability to Fibrillation

Previous studies showed that strong S_2 given during the RRP does not always induce repetitive responses or VF.[4] Hayashi et al.[13] simultaneously mapped V_m and Ca_i during a strong S_2 given during the RRP. The authors found that the induction of a Ca_i sinkhole is essential for a strong S_2 to induce repetitive responses or VF. However, the mechanism by which a Ca_i sinkhole triggers subsequent repetitive response is unclear. The present study documented that the timing of the $(dCa_i/dt)_{max}$ is coincidental with the onset of the first non-driven beat. These findings suggest that the I_{NCX} plays an important role in the initiation of the first repetitive beat. The participation of I_{NCX} in ventricular vulnerability suggests that triggered activity plays a role in the mechanisms of ventricular vulnerability. However, it is also possible that the availability of this electrogenic current lowered the depolarization threshold, allowing the surrounding wavefronts to reenter that site and cause an excitation. Therefore, the importance of I_{NCX} in ventricular vulnerability does not invalidate the idea that reentry underlies the mechanisms of ventricular vulnerability to S_2 [18–22]

Relevance to the Mechanisms of Ventricular Defibrillation

Efimov et al.[23–25] reported that a defibrillation shock can create virtual electrodes on the ventricles. These shock-induced virtual electrodes play important roles in the reinitiation of VF after a failed defibrillation shock. Hwang et al.[8, 26] simultaneously mapped V_m and Ca_i

after defibrillation shocks given during VF. They found that the postshock reinitiation of VF occurs from the Ca_i sinkhole, and that the reduced postshock Ca_i heterogeneity underlies the mechanisms by which biphasic waveform is superior to monophasic waveform in ventricular defibrillation. Based on the results of the present study, it is reasonable to hypothesize that these postshock virtual electrodes can cause differential Ca_i transients, with virtual anode sites generating larger Ca_i transients than at the virtual cathode sites.[13, 27] Hwang et al.[8] subsequently confirmed that there is postshock Ca_i heterogeneity after near-threshold defibrillation shocks. The first beat of postshock activation always occurs from the Ca_i sinkhole. The edge of the Ca_i sinkhole is a site with large spatial differences of Ca_i, a sign of increased I_{NCX} (Figure 1B). Consistent with the importance of increased I_{NCX} in generating first beat of postshock arrhythmias, the onset of Ca_i fluorescence preceded the onset of Vm at the first postshock activation sites.

Limitations

It is possible that intramural virtual cathodes exist and were not detected by our epicardial mapping techniques.[28] This limitation applies primarily to stimuli at high current strength, whereas during anodal dip, the current strength is low. Pharmacologic agents such as BAPTA-AM and substituting the Na^+ in the perfusate by Li^+ are not completely selective, and nonspecific effects cannot be excluded. Using a World Instrument A385 stimulator (the same as in the present study), Nikolski et al. [29] reported that a cathodal overshoot at the end of the anodal pulse was responsible for the appearance of anodal break excitation, since addition of a diode in the stimulator circuit eliminated both the overshoot and the break excitation. The authors suggested that a half-cell surface potential at the pacing electrode metal-saline interface may influence the pacing currents during unipolar anodal cardiac stimulation, creating break-like activation. According to this hypothesis, an initial anodal pulse de-excites the cell, facilitating subsequent excitation by the cathodal overshoot. Therefore, the anodal break-like excitation has a lower threshold than the cathodal make excitation. While this cathodal overshoot hypothesis can potentially explain the anodal break excitation, its effects are present throughout the diastole and are not limited to a small window of opportunity in late phase 3. Therefore, the cathodal overshoot by itself is insufficient to explain the presence of an anodal dip. Finally, strong stimuli can cause membrane electroporation, which may contribute to arrhythmogenesis. This limitation does not apply to the data obtained with near threshold current. Whether or not it affects the non-driven beats after S_2 is unclear.

Conclusion

Our study demonstrates that the anodal dip (supernormal) period results from a complex interplay of factors, among which the Ca_i transient plays a critical role by shaping the balance between depolarizing and repolarizing forces during late phase 3 to reduce the excitation threshold. Time of maximum I_{NCX} activation is also coincidental to the induction of non-driven beats from the Ca_i sinkhole after a strong premature stimulation, suggesting that I_{NCX} may play a role in ventricular vulnerability.

Acknowledgments

Names of grants: This study was supported in part by NIH Grants P01 HL78931, R01 HL78932, 71140, research grants (6-2009-0176, 7-2009-0583) of Yonsei University College of Medicine (BJ), Kawata and Laubisch endowments (JNW), an AHA Established Investigator Award (SFL), a Pauline and Harold Price Endowment and a Medtronic-Zipes Endowments (PSC). We thank Stephanie Plummer for her assistance.

References

1. Cranefield PF, Hoffman BF, Siebens AA. Anodal excitation of cardiac muscle. American Journal of Physiology. 1957; 190:383–390. [PubMed: 13458475]
2. Dekker E. Direct current make and break thresholds for pacemaker electrodes on the canine ventricle. Circ Res. 1970; 27:811–823. [PubMed: 5486248]
3. Chen PS, Wolf PL, Cha YM, Peters BB, Topham SL. Effects of subendocardial ablation on anodal supernormal excitation and ventricular vulnerability in open-chest dogs. Circulation. 1993; 87:216–229. [PubMed: 8419011]
4. Hoffman BF, Gorin EF, Wax FS, Siebens AA, Brooks CM. Vulnerability to fibrillation and the ventricular-excitability curve. American Journal of Physiology. 1951; 167:88–94. [PubMed: 14885473]
5. Piacentino V III, Weber CR, Chen X, Weisser-Thomas J, Margulies KB, Bers DM, Houser SR. Cellular basis of abnormal calcium transients of failing human ventricular myocytes. Circ Res. 2003; 92:651–658. [PubMed: 12600875]
6. Weber CR, Piacentino V III, Houser SR, Bers DM. Dynamic regulation of sodium/calcium exchange function in human heart failure. Circulation. 2003; 108:2224–2229. [PubMed: 14557358]
7. Fedorov VV, Lozinsky IT, Sosunov EA, Anyukhovsky EP, Rosen MR, Balke CW, Efimov IR. Application of blebbistatin as an excitation-contraction uncoupler for electrophysiologic study of rat and rabbit hearts. Heart Rhythm. 2007; 4:619–626. [PubMed: 17467631]
8. Hwang GS, hayashi H, Tang L, Ogawa M, Hernandez H, Tan AY, Li H, Karagueuzian HS, Weiss JN, Lin SF, Chen PS. Intracellular calcium and vulnerability to fibrillation and defibrillation in langendorff-perfused rabbit ventricles. Circulation. 2006; 114:2595–2603. [PubMed: 17116770]
9. Billman GE. Intracellular calcium chelator, bapta-am, prevents cocaine-induced ventricular fibrillation. AmJ Physiol. 1993; 265:H1529–H1535. [PubMed: 8238564]
10. Ogawa M, Lin SF, Weiss JN, Chen PS. Calcium dynamics and ventricular fibrillation. Circ Res. 2008; 102:e52. [PubMed: 18340012]
11. Bogdanov KY, Vinogradova TM, Lakatta EG. Sinoatrial nodal cell ryanodine receptor and na(+)-ca(2+) exchanger: Molecular partners in pacemaker regulation. Circ Res. 2001; 88:1254–1258. [PubMed: 11420301]
12. Blaustein MP, Lederer WJ. Sodium/calcium exchange: Its physiological implications. Physiol Rev. 1999; 79:763–854. [PubMed: 10390518]
13. Hayashi H, Lin SF, Joung B, Karagueuzian H, Weiss JN, Chen PS. Virtual electrodes and the induction of fibrillation in langendorff-perfused rabbit ventricles: The role of intracellular calcium. AmJPhysiol Heart Circ Physiol. 2008; 295:H1422–1428.
14. Chen PS, Joung B, Shinohara T, Das M, Chen Z, Lin SF. The initiation of the heart beat. Circ J. 2010; 74:221–225. [PubMed: 20019407]
15. Ranjan R, Tomaselli GF, Marban E. A novel mechanism of anode-break stimulation predicted by bidomain modeling. Circulation Research. 1999; 84:153–156. [PubMed: 9933246]
16. Ranjan R, Chiamvimonvat N, Thakor NV, Tomaselli GF, Marban E. Mechanism of anode break stimulation in the heart. Biophys J. 1998; 74:1850–1863. [PubMed: 9545047]
17. Shi W, Wymore R, Yu H, Wu J, Wymore RT, Pan Z, Robinson RB, Dixon JE, McKinnon D, Cohen IS. Distribution and prevalence of hyperpolarization-activated cation channel (hcn) mrna expression in cardiac tissues. Circ Res. 1999; 85:e1–6. [PubMed: 10400919]
18. Han J, Moe GK. Nonuniform recovery of excitability in ventricular muscle. Circulation Research. 1964; 14:44–60. [PubMed: 14104163]
19. Chen PS, Wolf PD, Dixon EG, Danieley ND, Frazier DW, Smith WM, Ideker RE. Mechanism of ventricular vulnerability to single premature stimuli in open-chest dogs. Circulation Research. 1988; 62:1191–1209. [PubMed: 2454762]
20. Pertsov AM, Davidenko JM, Salomonsz R, Baxter WT, Jalife J. Spiral waves of excitation underlie reentrant activity in isolated cardiac muscle. Circulation Research. 1993; 72:631–650. [PubMed: 8431989]

21. Lin SF, Roth BJ, Wikswo JP Jr. Quatrefoil reentry in myocardium: An optical imaging study of the induction mechanism. Journal of Cardiovascular Electrophysiology. 1999; 10:574–586. [PubMed: 10355700]
22. Eisner DA, Kashimura T, Venetucci LA, Trafford AW. From the ryanodine receptor to cardiac arrhythmias. Circ J. 2009; 73:1561–1567. [PubMed: 19667488]
23. Efimov IR, Cheng YN, Biermann M, Van WDR, Mazgalev TN, Tchou PJ. Transmembrane voltage changes produced by real and virtual electrodes during monophasic defibrillation shock delivered by an implantable electrode. Journal of Cardiovascular Electrophysiology. 1997; 8:1031–1045. [PubMed: 9300301]
24. Efimov IR, Cheng Y, Van Wagoner DR, Mazgalev T, Tchou PJ. Virtual electrode-induced phase singularity: A basic mechanism of defibrillation failure. Circulation Research. 1998; 82:918–925. [PubMed: 9576111]
25. Efimov I, Ripplinger CM. Virtual electrode hypothesis of defibrillation. Heart Rhythm. 2006; 3:1100–1102. [PubMed: 16945810]
26. Hwang GS, Tang L, Joung B, morita N, Kobayashi K, hayashi H, Karagueuzian HS, Weiss JN, Lin SF, Chen PS. Superiority of biphasic over monophasic defibrillation shocks is attributable to less intracellular calcium transient heterogeneity in langendorff-perfused rabbit ventricles. Journal of the American College of Cardiology. 2008; 52:828–835. [PubMed: 18755345]
27. Hayashi H, Kamanu SD, Ono N, Kawase A, Chou CC, Weiss JN, Karagueuzian HS, Lin SF, Chen PS. Calcium transient dynamics and the mechanisms of ventricular vulnerability to single premature electrical stimulation in langendorff-perfused rabbit ventricles. Heart Rhythm. 2008; 5:116–123. [PubMed: 18180025]
28. Sharifov OF, Fast VG. Role of intramural virtual electrodes in shock-induced activation of left ventricle: Optical measurements from the intact epicardial surface. Heart Rhythm. 2006; 3:1063–1073. [PubMed: 16945803]
29. Nikolski V, Sambelashvili A, Efimov IR. Anode-break excitation during end-diastolic stimulation is explained by half-cell double layer discharge. IEEE Trans Biomed Eng. 2002; 49:1217–1220. [PubMed: 12374349]

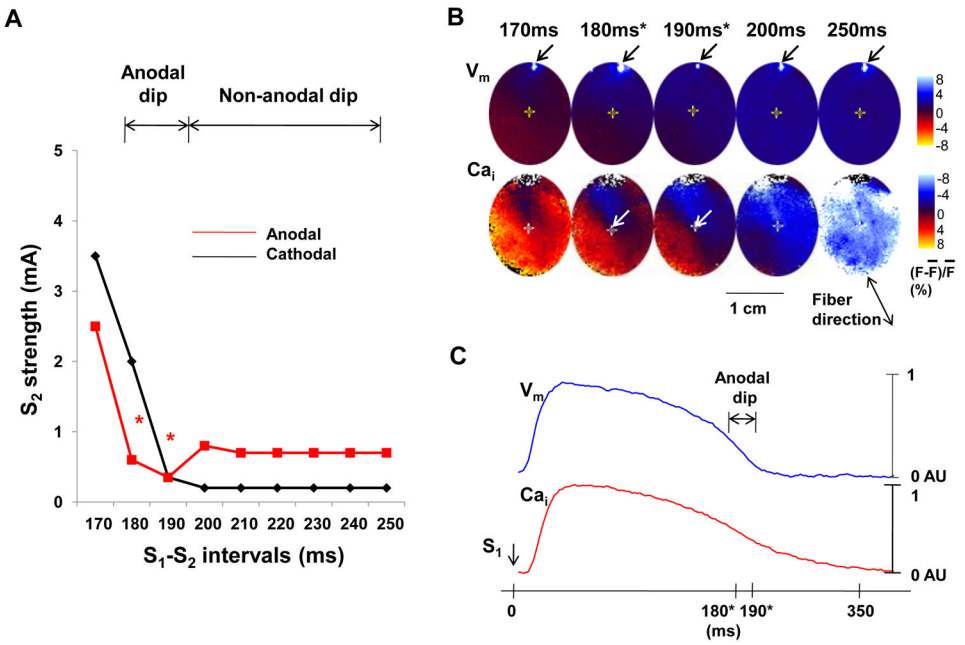

Figure 1.

V_m and Ca_i of the SI curve. A, SI curve of anodal and cathodal stimulation. The anodal threshold during anodal dip of 180–190 ms (asterisk) was lower than that of longer S_1-S_2 interval (non-anodal dip). B, Optical snapshots of V_m and Ca_i at the initiation of the S_2. The S_2 was located on the border zone between high (red) and low (blue) Ca_i during anodal dip (arrows). S_1 induced planar wave propagated from the upper left to lower right. The S_2 sites were indicated with the cross mark. The numbers above optical snapshots indicate the S_1-S_2 coupling interval. The white spot in each V_m snapshot was produced by the flash of a LED lamp used to document the timing of the S_2. C, V_m and Ca_i tracings recorded at the S_2 (the cross mark in B) during S_1 pacing of 350ms. Note that the S_2 occurred at the junction between red and blue areas during the anodal dip (180 ms and 190 ms), indicating that the anodal dip occurred at sites with rapidly changing Ca_i.

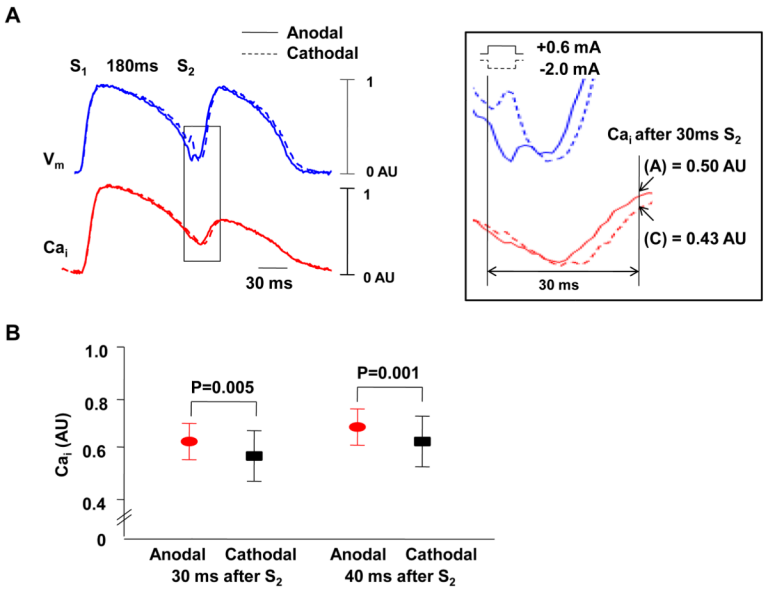

Figure 2.

Ca_i elevation after anodal and cathodal S_2. A, 0.6 mA anodal and 2.0 mA cathodal stimuli during anodal dip (S_1-S_2 interval of 180 ms). The boxed region was magnified to show that the Ca_i level is higher after anodal (A) than cathodal (C) stimulus. The cathodal stimulus is followed by immediate depolarization (broken red arrow) while the anodal stimulus resulted in hyperpolarization followed by depolarization (solid red arrow). Because there was a 6 ms pulse width, the break excitation of the anodal stimulus excites the tissue during a more recovered phase of the action potential, leading to shorter stimulus-response latency and earlier rise of phase 0 than the make excitation associated with cathodal stimulus.B, Ca_i 30 ms and 40 ms after S_2. The Ca_i transient measured 30 ms and 40 ms after anodal S_2 was significantly higher than that of cathodal stimulus (P=0.005 and 0.001, respectively).

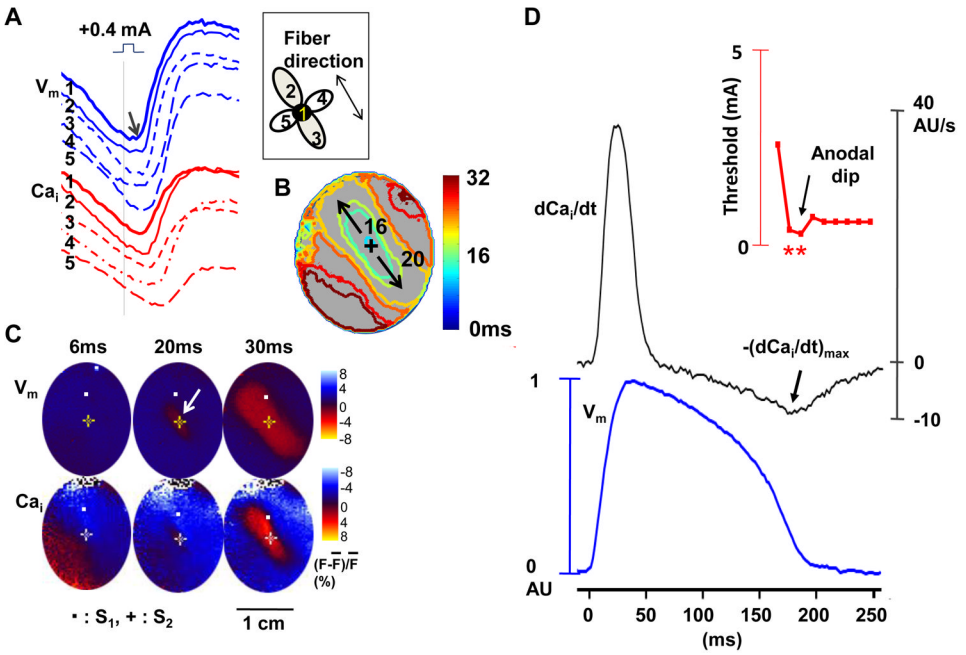

Figure 3.

The anodal-break excitation and role of Ca_i removal during anodal dip. A through C show a typical example of anode-break excitation originating from the stimulation site itself during anodal stimulus of 0.4 mA at the anodal dip period (S_1-S_2 interval of 190 ms). A, V_m and Ca_i tracings from S_2 site (site 1) and surrounding 4 sites (sites 2–5). B, V_m isochronal map with times of activation (in ms) marked on selected isochrones, with the onset of S_2 as time zero. C, Corresponding V_m and Ca_i fluorescence snapshots. Note that the excitation started from the site of S_2 (arrow) and propagated faster along the fiber direction than across the fiber direction. D, The anodal SI curve (upper panel), dCa_i/dt (middle panel) and simultaneous V_m traces (lower panel) for S_1-paced beats at the S_2 site. The dCa_i/dt values were the highest during phase 1 and the lowest during the phase 3 of the action potential. $-(dCa_i/dt)_{max}$ (arrow) occurred when S_1-S_2 coupling interval was 180 ms, which was during the anodal dip on the SI curve.

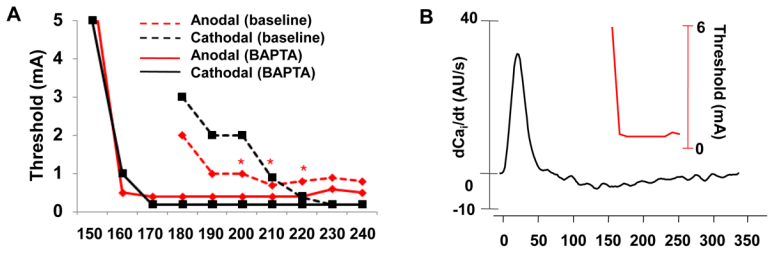

Figure 4.

The effect of BAPTA-AM on the anodal SI curve. A, The SI curve before (broken lines) and after (solid lines) BAPTA-AM (20 μmol/L) infusion. B, The anodal SI curve and dCa_i/dt after BAPTA-AM infusion. The anodal dip was eliminated by BAPTA-AM infusion in all ventricles.

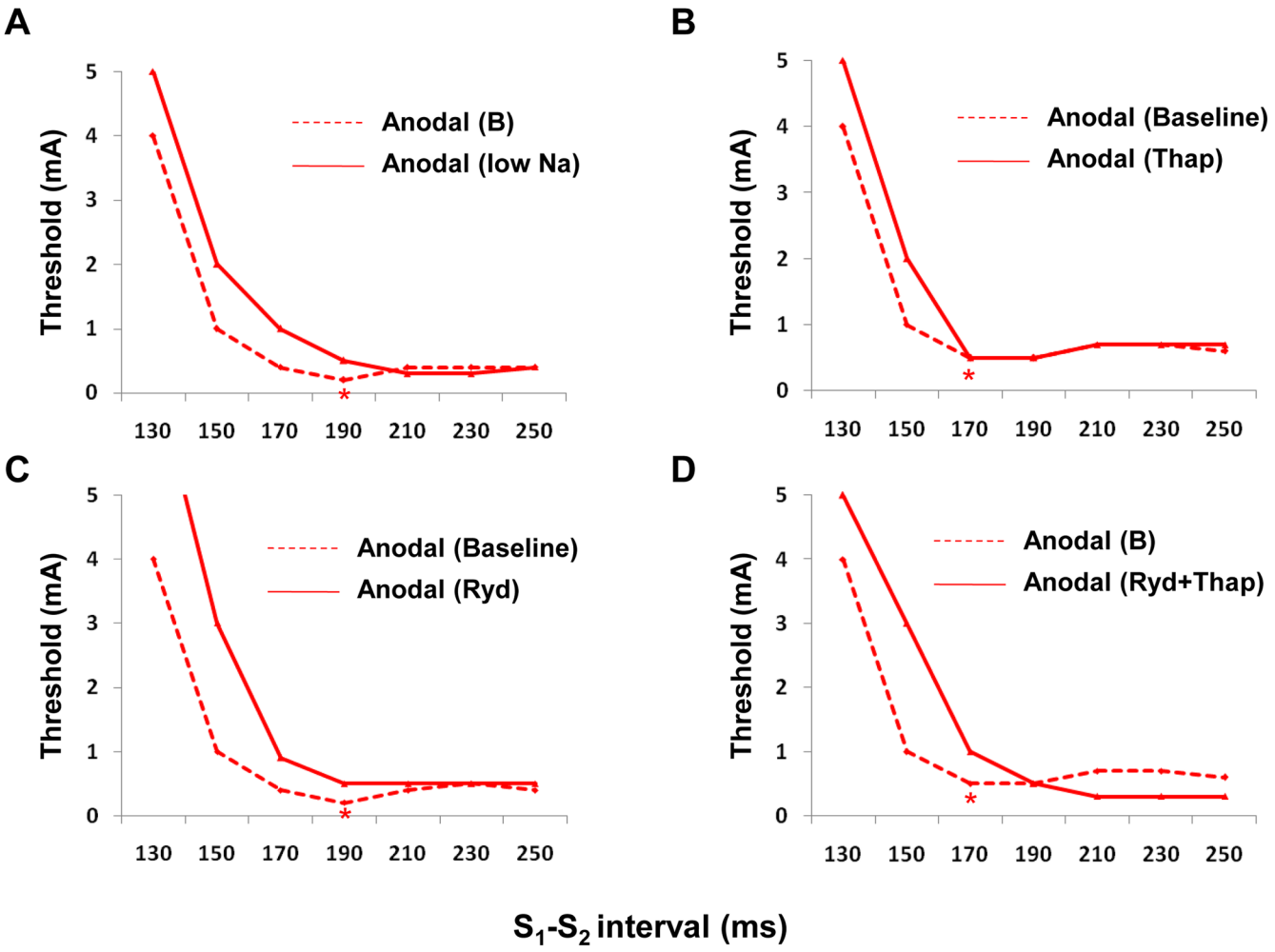

Figure 5.
The anodal SI curves after other pharmacological interventions. A, Before (broken lines) and after (solid lines) infusion of low Na. Anodal dip disappeared after low Na. B, Thapsigargin (Thap, 3 μmol/L). C, Ryanodine (Ryd, 3 μmol/L). D, Ryanodine (3 μmol/L) and thapsigargin (3 μmol/L). Asterisks indicate anodal dip.

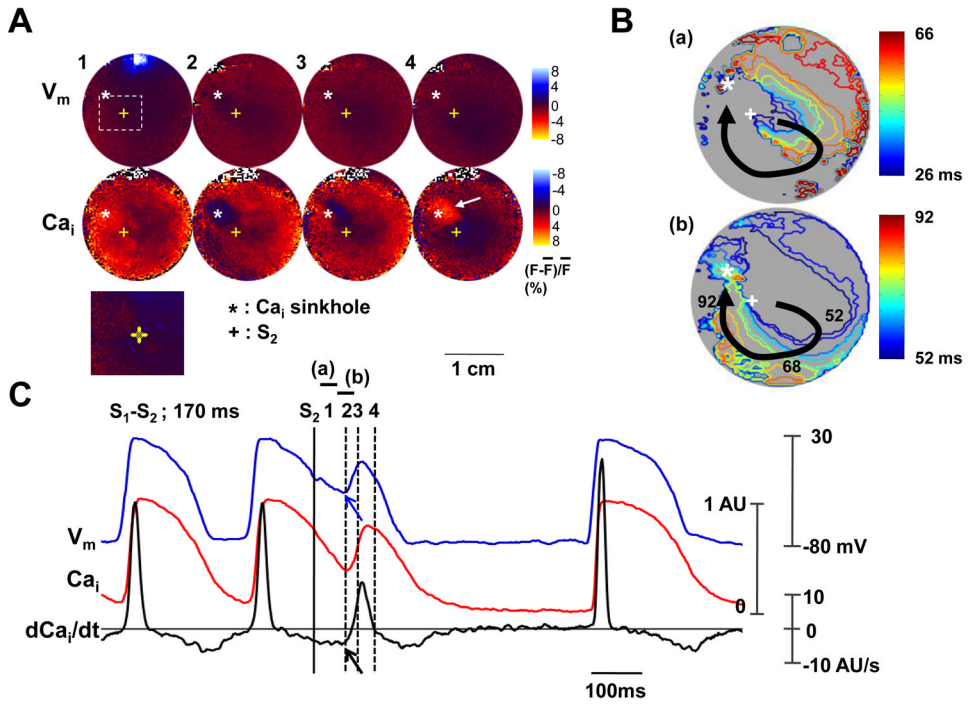

Figure 6.

The role of maximum Ca_i removal rate in Ca_i sinkhole and activation. The 10 mA anodal S_2 during S_1-S_2 interval of 170 ms. A, V_m and Ca_i fluorescence snapshots. Note that Ca_i elevation starts from the margin of Ca_i sinkhole (asterisks) and propagates to the entire sinkhole (arrow). Lower panel is the magnified image of boxed region. B, V_m isochronal map with times of activation (in ms) marked on selected isochrones, with the onset of S_2 as time zero. C, V_m tracing, Ca_i tracing and dCa_i/dt recorded from the Ca_i sinkhole.

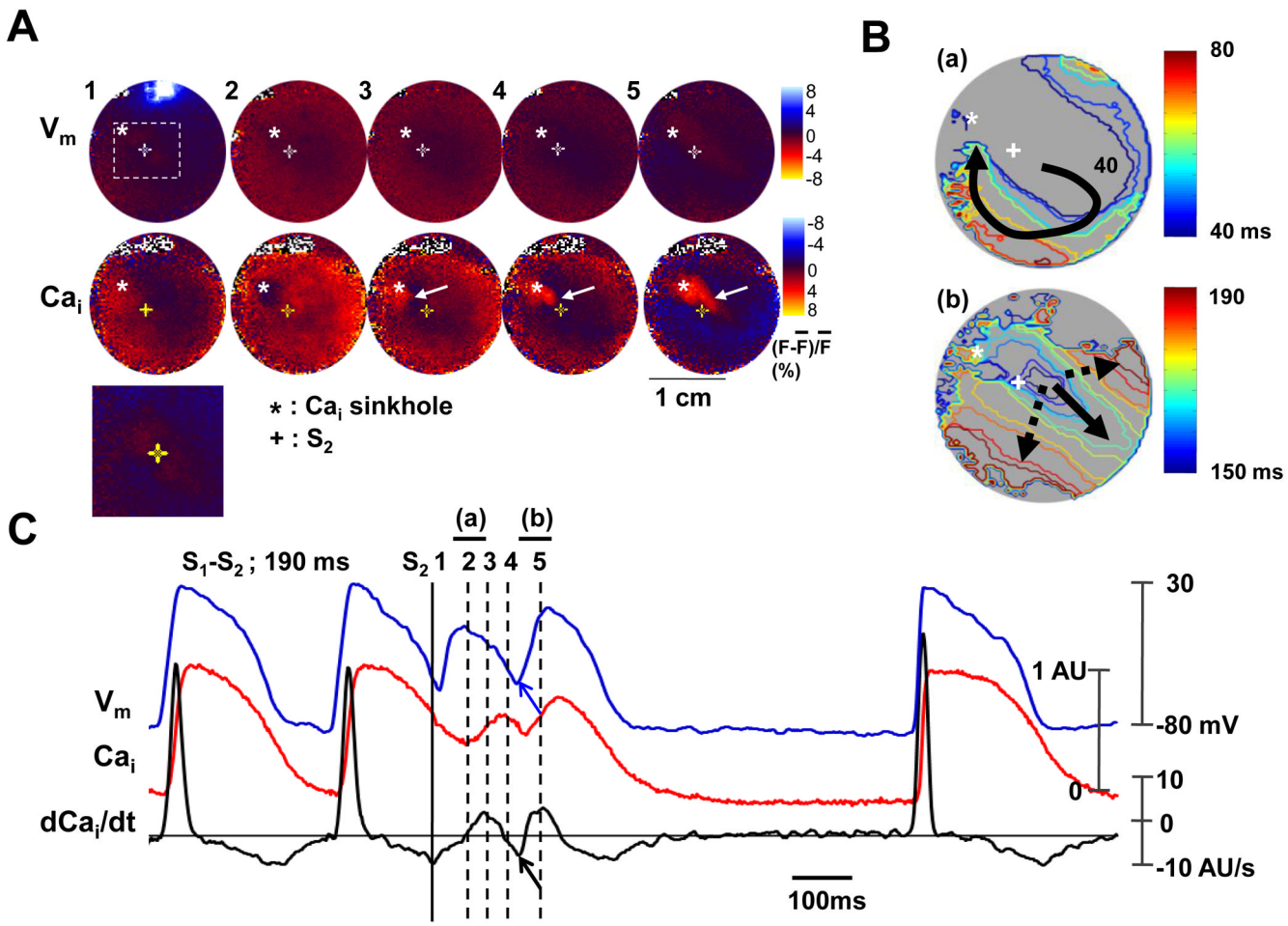

Figure 7.

The role of maximum Ca_i removal rate during repetitive beat. The 10 mA anodal S_2 during the S_1-S_2 interval of 190 ms. A, V_m and Ca_i fluorescence snapshots. Note that Ca_i elevation starts from the Ca_i sinkhole (asterisks) and propagates slowly to other sites (arrow). Lower panel is the magnified image of boxed region. B, V_m isochronal map with times of activation (in ms) marked on selected isochrones, with the onset of S_2 as time zero. C, V_m tracing, Ca_i tracing and dCa_i/dt recorded from the Ca_i sinkhole.

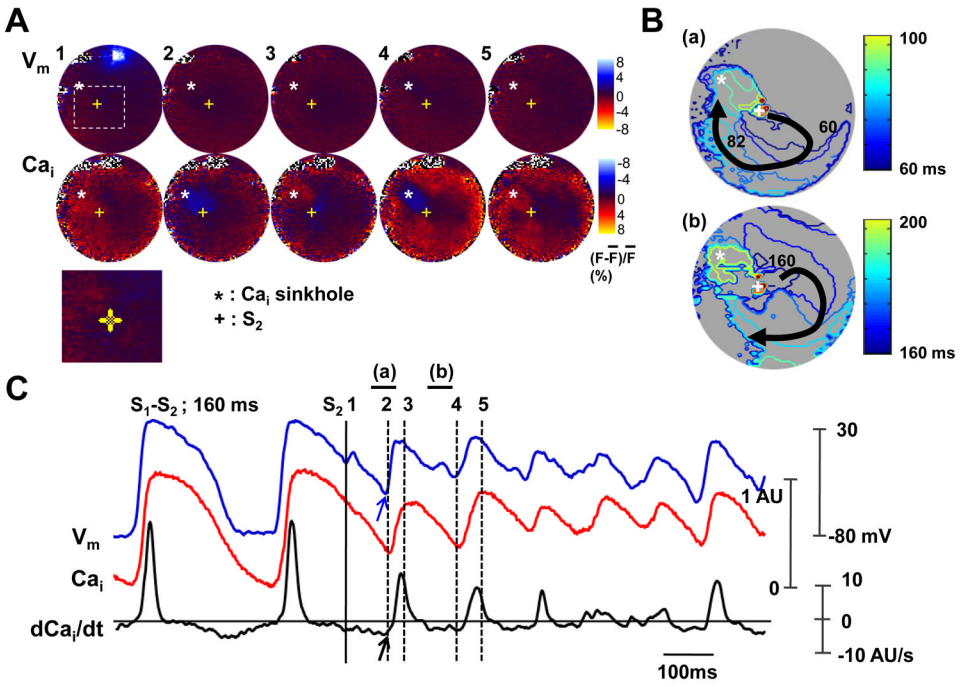

Figure 8.

The role of maximum Ca_i removal rate during ventricular fibrillation induced by an anodal S_2 (30 mA) given 160 ms after the last S_1. A, V_m and Ca_i fluorescence snapshots. Note the Ca_i sinkhole (asterisk) and Ca_i elevation (arrow). Lower panel is the magnified image of boxed region. B, V_m isochronal map with times of activation (in ms) marked on selected isochrones, with the onset of S_2 as time zero. C, V_m tracing, Ca_i tracing and dCa_i/dt recorded from the Ca_i sinkhole.